Functionalized tungsten disulfide nanotubes for dopamine and catechol detection in a tyrosinase-based amperometric biosensor design

Quentin Palomar, Chantal Gondran, Jean-Paul Lellouche, Serge Cosnier, Michael Holzinger

ARTICLE

Functionalized Tungsten disulfide nanotubes for Dopamine and Catechol detection in a Tyrosinase-based Amperometric Biosensor design

Received 00th January 20xx,
Accepted 00th January 20xx

DOI: 10.1039/x0xx00000x

Quentin Palomar, [a] Chantal Gondran†, [a] Jean-Paul Lellouche, [b] Serge Cosnier, [a] and Michael Holzinger†, [a]

WS_2 nanotubes functionalized with carboxylic acid functions (WS_2-COOH) were used for improved immobilization of the enzyme tyrosinase in order to form an electrochemical biosensor towards catechol and dopamine. The nanotubes were deposited on glassy carbon electrodes using a dispersion-filtration-transfer procedure to assure the reproducibility of the deposits. After the electrochemical and morphological characterization of these WS_2-COOH nanotubes deposits, the formed biosensors showed very satisfying performances towards catechol detection with a linear range between 0.6 – 70 µmol L^{-1} and a sensitivity of 10.7 ± 0.2 mA L mol^{-1}. The apparent Michaelis Menthen constant of this system is slightly lower than the K_M value of tyrosinase in solution reflecting an excellent accessibility of the active site of the enzyme combined with a good mass transport of the target molecule through the deposit. For dopamine detection, we observed an accumulation of this substrate due to electrostatic interactions between the dopamine's amine function and the carboxylic acid groups of the nanotubes. This led to improved signal capture at low dopamine concentrations. With a linear range between 0.5 – 10 µmol L^{-1} and 10 – 40 µmol L^{-1}, and respective sensitivities of 6.2 ± 0.7 mA L mol^{-1} and 3.4 ± 0.4 mA L mol^{-1}, the overall sensor performances are in the average of comparable results using carbon nanotubes. Nonetheless, the simplified handling of these nanotubes and their reduced environmental impact make these WS_2-COOH nanotubes a promising nanomaterial for biosensing applications.

Introduction

Nanomaterials are nowadays essential tools in biosensor research not only due to the enhanced surface area but also to a variety of particular phenomena related to the nanosized structure [1-3]. Within the vast availability of different nanomaterials, carbon nanotubes [4, 5] and later graphene [6, 7] became prominent candidates for biosensing applications because of their beneficial electronic and optical properties for enhanced signal capture of the biological recognition event. More recently, 2D transition metal dichalcogenides such as WS_2 and MoS_2 showed promising properties in biosensor designs [8] which are principally based on the layered form of these metal dichalcogenides. The detection of the target is commonly transduced via optical detection [9] or in a field effect transistor design [10] but such dichalcogenides have also shown their appropriateness in electrochemical biosensor setups [11]. The synthesis of WS_2 and MoS_2 can also form differently shaped materials like nanotubes or nanorods [12, 13] with improved surface activities and might be more appropriate for biosensor applications [14]. Raichman et al. reported an efficient functionalization method for tungsten disulfide inorganic nanotubes using a highly electrophilic acidic Vilsmeier-Haack reagent for homogeneous covalent carboxylation of the WS_2 walls. The carboxylic acid functions lead to improved dispersions in aqueous media and represent efficient anchor groups for the immobilization of bioreceptor units [15, 16]. Furthermore, the clearly reduced cytotoxicity of such transition-metal dichalcogenides compared to carbon nanomaterial represents an advantage when combined with biological entities [17, 18]. In this work, we used such carboxylated WS_2 (WS_2-COOH) nanotubes for the immobilization of the tyrosinase enzyme as protein model and evaluated this sensor for the detection of catechol and dopamine.

Catechol (CA) is a toxic compound [19] but serves as starting materials for the synthesis of many different chemicals and therein a wide variety of pesticides [20]. This compound therefore contributes to the pollution of soils and groundwater. It further has a low degradation rate which worsens its environmental impact.

[a] Univ. Grenoble Alpes, CNRS, DCM UMR 5250, F 38000, Grenoble, France
[b] Bar Ilan University, Ramat Gan, 5290002, Israël

† corresponding authors: chantal.gondran@univ-grenoble-alpes.fr, michael.holzinger@univ-grenoble-alpes.fr

Dopamine (DA) is a neurotransmitter and plays an important role as an extracellular chemical messenger in the cardiovascular, renal, hormonal and nervous systems. It is at the centre of cell signal transmission and has therefore a strong influence on human behaviour. Abnormal concentrations of DA in biological fluids are an indicator of several diseases such as schizophrenia, Huntington's disease or Parkinson [21, 22]. An efficient filtration and transfer technique [23] to form identic WS_2-COOH nanotube deposits was adjusted for the electro-enzymatic detection of these two compounds. As illustrated in Scheme 1, the carboxylic acid groups served as anchor for the immobilization of tyrosinase, an enzyme that oxidises specifically catechol and dopamine to its respective quinones. These quinones are then monitored at cathodic potentials via electrochemical reduction to the initial hydroquinones. The WS_2-COOH nanotubes serve here principally as porous nanostructures on the working electrodes to immobilize and enhanced amount of tyrosinase enzymes.

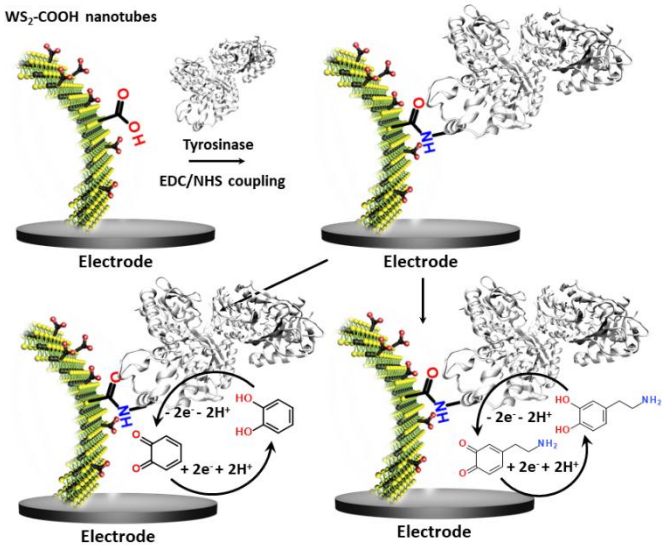

Scheme 1: Sketch of the functionalization of WS_2 modified glassy carbon electrodes with the enzyme tyrosinase via a standard EDC/NHS coupling reaction. These modified bioelectrodes served for the detection of catechol (bottom left) and dopamine (bottom right) at –O.2 V vs Ag^+/Ag.

Results and discussion

Characterization of the WS_2-COOH nanotubes

Before the construction of the biosensor, the morphology and electrochemical behaviour of the WS_2-COOH nanotubes were characterized. Figure 1 shows the scanning electron microscopy images of these nanotubes as synthesized (Figure 1A, B) and after film formation and transfer on GCE (Figure1 C, D). At the same magnification (Figures 1A and C), the as synthesized WS_2-COOH nanotubes and the formed film do not show significant differences and demonstrate that the stirring dispersion, filtration and transfer procedure does not affect these nanotubes.

The length of these nanotubes is comprised between 2 and 10 microns for a diameter of about 100 to 200 nm. It also seems that the WS_2-COOH nanotubes are formed of rolled-up WS_2 sheets. This lamellar structure is particular visible at higher magnification as shown in Figure 1B. Figure 1D shows the deposits at lower magnification and reveals an assembly of randomly oriented nanotubes forming a highly porous structure.

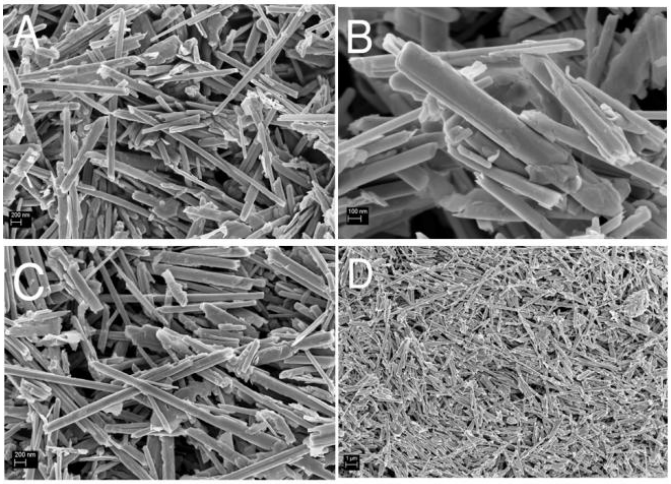

Figure 1: SEM images of A-B) as synthesized WS_2-COOH powder at a magnification of A) ×20000, and B) 50000. SEM images of C-D) thin films of WS_2-COOH nanotubes at a magnification of C) ×20000, and D ×5000.

To determine the thickness and roughness of the formed WS_2-COOH films, a confocal laser microscope was used. This technique allows mapping the height and the morphology of the films by profilometry. Figure 2 shows images taken at the boundary between the gold substrate and the WS2-COOH films.

A thickness of 6.2 µm was determined for a roughness of ± 0.6 µm. This relatively high roughness, 10% of the total thickness, can be explained by the highly porous nature of the formed film. Finally, it appears that thickness and roughness values for 3 different films, exhibit a relative standard deviation of 6% and 3.6% respectively highlighting the reproducibility of the procedure.

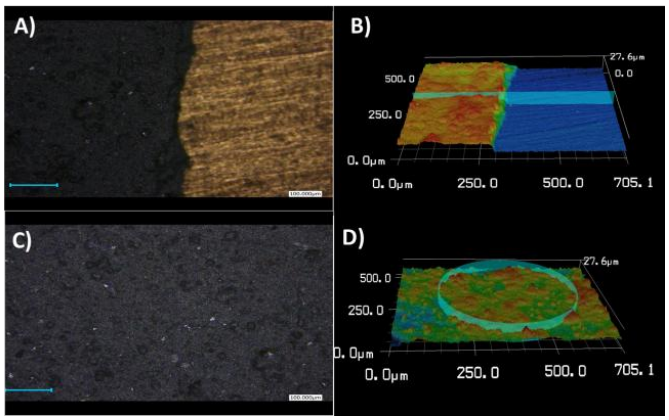

Figure 2: Height mapping images and 3D views realized with a confocal laser microscope at a magnification of × 50 of WS_2–COOH film at the cut edge (A and B) with

the film on the left and the substrate on the right. C and D, Microscope image of the center of the film (C and D).

The electrochemical behaviour of these films on GCEs was studied using cyclic voltammetry in organic media (Figure 3). Within a scan range between -2.0 and +2.0 V vs Ag+/Ag, the first cycle shows a strong and large irreversible anodic peak at 1.7 V that starts at 0.6V. This peak almost disappears during the second scan. According to the studies about the inherent electrochemistry of transition-metal dichalcogenides by Bonde et al.[24], this peak can be assigned to the irreversible oxidation of WS_2 on surface forming WO_4^{2-}. The potential shift in the second scan is related to the oxidation of remaining WS_2 in a WO_4^{2-} environment. At the reverse scan towards negative potentials, an irreversible cathodic peak was observed at -0.7 V which also disappeared at the second scan. Here, it is more likely that loosely adsorbed species are released during the first scan or a reduction of the protons since WS_2 can be used as electrocatalysts for hydrogen evolution reaction (HER) [25]

Most important, the WS_2–COOH nanotubes are electrochemically silent in the potential range around -0.2 V where should occur the amperometric detection of dopamine and catechol with the tyrosinase based biosensor. Unfortunately, films of WS_2-COOH are almost not conductive at this potential ($1.6 \pm 0.1 \times 10^{-07}$ S cm^{-1}, measured using a four-point probe) and can therefore not be considered as extension of the electrode.

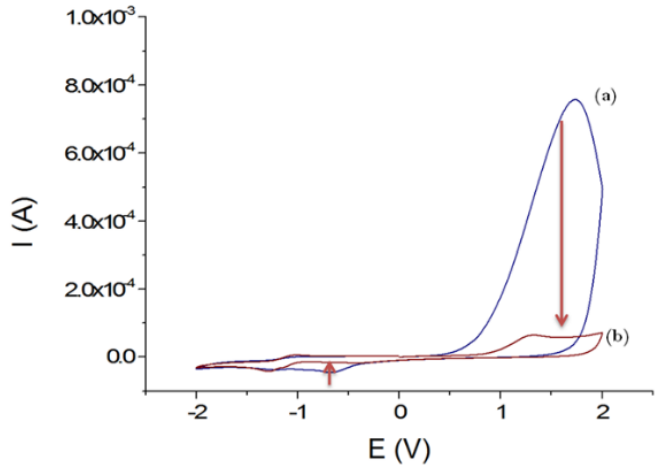

Figure 3: Voltammograms obtained in CH_3CN + 0.1 mol L^{-1} TBAP; first cycle (a) and second cycle (b) with the GCE/WS_2-COOH modified electrode between -2.0 and +2.0 V vs Ag^+/Ag; Scan rate: 100 mV s^{-1}.

Detection of catechol

The detection of catechol using tyrosinase is based on the enzymatic oxidation of phenols and o-bisphenols like catechol to o-quinones. The product of the enzymatic reaction is then reduced at the electrode at -0.2 V vs SCE. The resulting chronoamperometric current density is proportional to the analyte concentration. In addition, the target molecule is regenerated during the reduction at the electrode which allows the amplification of the electrochemical signal and leads to increased sensitivity [26, 27]. The measurements were done by immersing the modified electrode in an electrochemical cell containing 20 mL of PBS (0.1 mol.L^{-1}, pH = 7.4).

Figure 4A shows the increase of steady-state current response of the bioelectrode upon successive additions of catechol and illustrates the fast response time (3s). Figure 4B shows the amperometric response of the bioelectrode as a function of catechol concentration in the range of 0.3-220 µmol L^{-1} resulting in a calibration curve which follows a Michaelis-Menten kinetic.

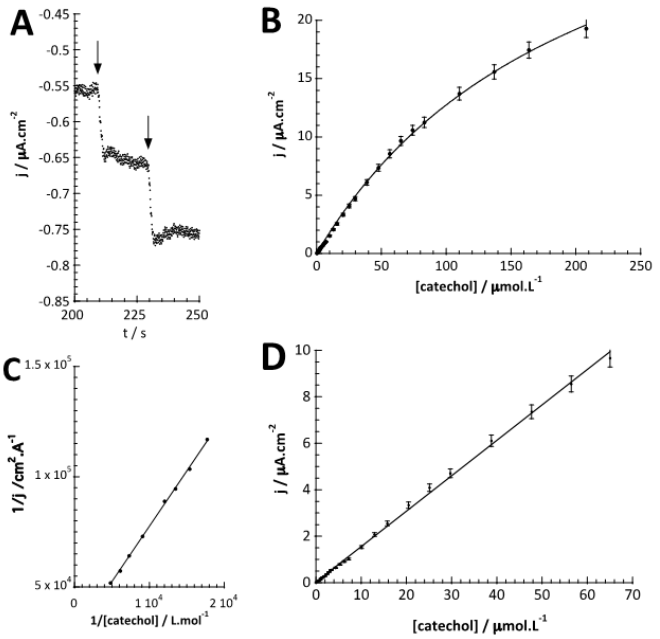

Figure 4: A) Chronoamperometric response of the GC/WS_2-COOH/tyrosinase electrode (E = -0.2 V vs. SCE; 0.1 mol L^{-1} PBS; pH 7.4) for successive increase of catechol concentration from 0.3 µmol L^{-1} to 220 µmol L^{-1}. B) Plot of the current density towards catechol concentration on Tyrosinase/WS_2-COOH/GCE. C) Lineweaver-Burk plot of the corresponding data. D) Plot of the linear part of the current density towards increasing catechol concentrations.

The maximum current density, j_{max}, is related to the amount of immobilized enzymes on the electrode surface and to the affinity of the enzyme for its target and thus to the apparent Michaelis-Menten constant (K_M^{app}). The linear fit equation ($R^2 = 0.99897$) obtained with the Lineweaver-Burk representation leads to 36 µA cm^{-2} and 183 µmol L^{-1} for j_{max} and K_M^{app}, respectively (Figure 4C):

$$\frac{1}{j} = \frac{1}{j_{max}} + \frac{K_M^{app}}{j_{max} \times [catechol]} = 27406 + \frac{5.015}{[catechol]}$$

The K_M^{app} used here reflects the kinetics of the immobilized enzyme and not that of the free enzyme in solution. Surprisingly, the determined K_M^{app} is slightly lower than the K_M of free enzymes (300 µmol L^{-1} with catechol [28]) in spite of the constraints to the mass transport at immobilized states. Nevertheless, this behaviour is quite common and was already observed with tyrosinase biosensors [29, 30]. To explain this phenomenon, it is necessary to consider the formula for K_M:

$$K_M = \frac{k_{-1} + k_2}{k_1}$$

Where k_1 represents the kinetic of the enzyme-substrate complex formation and k_2 the transformation of enzyme-substrate complex into the product of the enzymatic reaction and the regenerated enzyme. This formula for K_M does not take into account the co-substrate (oxygen) concentration of the enzymatic reaction but this is actually the case since tyrosinase reduces oxygen to water to regenerate itself. By integrating the co-substrate concentration in the equation for k_2 ($k_2 = k_2° \times [O_2]$), K_M^{app} can be calculated:

$$K_M{}^{app} = \frac{k_{-1} + k_2°[O_2]}{k_1}$$

Thus, the value of K_M^{app} is directly related to the oxygen concentration. However, the use of nanomaterials considerably increases the quantity of immobilized enzymes and the co-substrate amount is rapidly consumed. Since the oxygen supply is limited by diffusion, a concentration gradient of oxygen can thus be established between the solution and the enzyme. The co-substrate concentration in the enzyme's environment is then lower than in solution and results in a decrease of K_M^{app} since the value of k_2 is lower than expected. Assuming that the enzyme is here in a favorable environment, it may then be assumed that the oxygen concentration decreases to 40% close to the enzymes compared to the rest of the solution.

The linear part of the calibration curve within the concentration range between 0.6 µmol.L^{-1} and 70 µmol.L^{-1} reveals a sensitivity value of 152.5 mA L cm^{-2} mol^{-1} (R^2 = 0.9986).It should be noted that the linearity range and the sensitivity are identic for the two electrodes. The electrochemical characteristics in terms of molecular architecture, K_M^{app}, maximum current density, linearity, and sensitivity are summarized in Table 1.

The linearity range of our system are similar to those found in literature [35]. This can be explained by the presence of WS_2-COOH nanotubes which allows a high amount of immobilized enzymes on the electrode surface as other nanomaterials. However, the sensitivity remains relatively low compared to other reports [34]. This can be due either to the rapid oxygen consumption and/or to reduced permeability of the WS_2-COOH film but finally results most likely from the almost inexistent conductivity at this potential.

Table 1: Comparison of the characteristics (system used, K_{Mapp}, i_{max}, linearity and sensibility) of different nanostructured electrochemical catechol biosensors.

	System used	K_{Mapp} / µmol L^{-1}	i_{max} / µA	Linearity/ µmol L^{-1}	Sensitivity / mA L mol^{-1}
This work	WS_2-COOH nanotube + GCE	183 ± 20	2.5 ± 0.6	0.6 - 70	10.7 ± 0.2
Karim et al. [31]	Gold nanoparticule + screen printed carbon electrode	-	-	0.01 - 80	13720
Sethuraman et al. [32]	PEDOT-rGO+ GCE	30.48	92	0.04 - 62	1600
Zhou et al. [33]	Mesoporous carbon nitride + GCE	11.07	11.07	0.05 - 12.5	593
Bujduveanu et al. [34]	CNT + $CaCO_3$ nanoparticules + GCE	7	39.2	0 - 8	2500
Mei et al. [35]	rGO–PdCu Nanocage + GCE (laccase)	-	-	500 - 1155 1655 - 5155	12.65 5.51

Detection of dopamine

As for catechol, tyrosinase also oxidizes dopamine to dopamine-o-quinone which can be detected at the same potential (-0.2 V vs SCE). The detection of dopamine was thus performed under identic conditions as described above. Figure 5A illustrates the chronoamperometric response of the modified GC/WS_2-COOH/tyrosinase electrodes as a function of the dopamine concentrations. It can be seen that the current stabilizes rapidly after dopamine injection confirming the fast electronic transfer and the permeation of the substrate through the WS_2-COOH nanotube deposit. The range of concentrations tested varies from 0.5 µmol L^{-1} to 137 µmol L^{-1}. From the shape of the curve, it seems that the dopamine oxidation via tyrosinase is also governed by Michaelis-Menten kinetics. Figure 5B shows the evolution of the current density as a function of the dopamine concentration. The observed maximum current density is clearly higher than for catechol detection.

This may be due to the fact that the amine function of dopamine is partially positively charged at pH 7.4 and hence can display a faster and deeper penetration inside the WS2-COOH matrix which is negatively charged. As a consequence, the calibration curve, which is obtained by plotting the current density as a function of the dopamine concentration in solution, does not necessarily reflect the dopamine concentration in the WS2-COOH matrix.

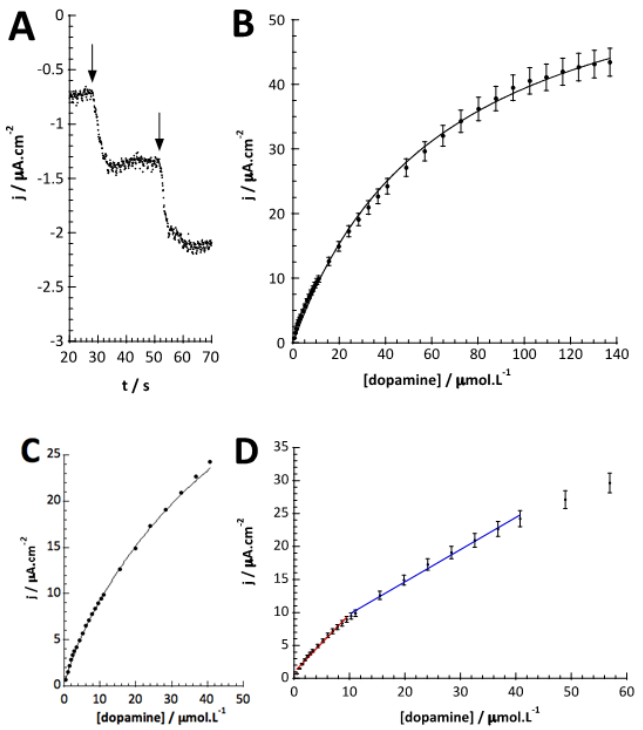

Figure 5: A) Chronoamperometric response of the GC/WS_2-COOH/tyrosinase electrodes (E= -0.2 V vs. SCE; 0.1 mol L^{-1} PBS; pH 7.4) for increasing dopamine concentrations from 0.5 µmol L^{-1} to 137 µmol L^{-1}, B) Plot of the current density towards dopamine concentrations. C) Fit of the calibration curve with the Michaelis-Menten equation taking into account the accumulation of dopamine in the biosensor matrix. D) Plot of linear parts of the current density towards increasing dopamine concentrations measured with GC/WS_2-COOH/tyrosinase electrode.

From the Lineweaver-Burk representation (not shown), a K_M^{app} of 41 µmol L^{-1} and j_{max} of 57 µA cm^{-2} could be determined following the linear fit equation (R^2 = 0.99344):

$$\frac{1}{j} = \frac{1}{j_{max}} + \frac{K_M^{app}}{j_{max} \times [dopamine]} = 17614 + \frac{0.72938}{[dopamine]}$$

The maximum current density, j_{max}, is higher for the detection of dopamine (57 µA cm^{-2}) than for the detection of catechol (36 µA cm^{-2}) at the same amounts of enzymes. It seems that the WS_2-COOH nanotubes provide a better accessibility to the enzyme for the dopamine rather than for catechol.

The experimental K_M^{app} value is, as for the catechol experiments, lower than the K_M of the free enzyme (K_M = 2.2 mmol L^{-1} for the tyrosinase towards dopamine) [28] related to the limited oxygen concentration. It should be noted that the experimentally determined K_M^{app} is lower for dopamine (41 µmol L^{-1}) than for catechol (183 µmol L^{-1}). In solution, the K_M value of tyrosinase for dopamine is higher (2.2 mmol L^{-1}) compared to catechol (300 µmol.L^{-1}). This inversion may be related to an accumulation of dopamine in the WS_2-COOH matrix related to electrostatic interactions. This can be deduced by the arc shaped (and not linear) calibration curve at low dopamine concentrations. In order to estimate this accumulation effect, we fitted this part of the calibration curve in Figure 5C using an equation that takes the concentration change of dopamine into account:

$$\mathrm{DA}_{(\text{in solution,positive charge})} + \text{negative charge (NC)}_{(\text{on } WS_2\text{–COOH})} \rightleftharpoons \mathrm{DA}_{(\text{accumulated})}$$

at the equilibrium:

$$K_d = \frac{[\mathrm{DA}] \times [\mathrm{NC}]}{[\mathrm{DA}]_{acc}}$$

with K_d as the equilibrium dissociation constant. [DA], [NC] and $[DA]_{acc}$ are the dopamine concentrations in solution, negative charges on WS_2-COOH nanotubes, and accumulated dopamine in the deposit, respectively. The unknown amount of negative charges on WS_2-COOH can be substituted by the difference between the maximum accumulating dopamine concentration, $[\mathrm{DA}]_{acc}^{max}$ and the actually accumulated dopamine concentration, $[DA]_{acc}$.:

$$K_d = \frac{[\mathrm{DA}] \times ([\mathrm{DA}]_{acc}^{max} - [\mathrm{DA}]_{acc})}{[\mathrm{DA}]_{acc}}$$

Leading for $[DA]_{ads}$ to:

$$[\mathrm{DA}]_{acc} = \frac{[\mathrm{DA}] \times [\mathrm{DA}]_{acc}^{max}}{K_d + [\mathrm{DA}]}$$

The integration of this equation inside the Michaelis-Menten equation gives:

$$j = \frac{j_{max} \times \left(\frac{[\mathrm{DA}] \times [\mathrm{DA}]_{acc}^{max}}{K_d + [\mathrm{DA}]}\right)}{K_M^{app} + \left(\frac{[\mathrm{DA}] \times [\mathrm{DA}]_{acc}^{max}}{K_d + [\mathrm{DA}]}\right)}$$

By fitting the first part of the calibration curve with this equation (figure 5C, R^2 = 0.99728), the dissociation constant, K_d, is estimated at 5×10^{-5} and the maximum accumulating dopamine concentration, $[\mathrm{DA}]_{acc}^{max}$, at 35 µmol L^{-1}. It can therefore be concluded that below the value of 35 µmol L^{-1}, the dopamine concentration is greater around the enzymes than in solution. At higher values, the dopamine concentration is the same in the WS_2-COOH matrix and in solution.

Figure 5D shows that at low dopamine concentration, the calibration curve presents two successive linear parts as other examples reported in literature for PPO biosensors [36-38]. For a concentration range varying from 0.5 to 10 µmol L^{-1}, the biosensor sensitivity for dopamine is 88.0 mA L cm^{-2} mol^{-1} (or 6.2 mA L mol^{-1}) and 48.8 mA L cm^{-2} mol^{-1} (or 3.4 mA L mol^{-1}) between 10 and 40 µmol L^{-1} of dopamine. This setup and phenomena are quite good reproducible with a relative standard deviation of 4.8% for three different electrodes.

Table 2 compares our findings with representative examples found in literature about dopamine detection using tyrosinase combined with a nanomaterial focusing various criteria such as sensitivity, linearity, the maximum current densities and the calculated K_M^{app}. The system presented here has slightly lower performances in terms of linearity range, sensitivity, and limit of detection compared to carbon nanotubes (CNTs), widely used for biosensing application, despite good maximum current densities.

Table 2: Comparison of the obtained characteristics (system used, K_M^{app}, imax, linearity and sensibility) of different nanostructured electrochemical dopamine biosensors.

	System used	K_M^{app} / µmol L^{-1}	i_{max} / µA	Linearity/ µmol L^{-1}	Sensitivity / mA $L\ mol^{-1}$
This work	WS_2-COOH nanotube + GCE	41 ± 2	4 ± 0.5	0.5 - 10 10 - 40	6.2 ± 0.7 3.4 ± 0.4
Bujduveanu et al. [34]	CNT + $CaCO_3$ nanoparticules + GCE	30	-	0.015 - 30	250
Wang et al. [39]	SiO_2 nanoparticule+ acide phytic + GCE (laccase)	-	-	0.99 - 103.1	1.9
Lete et al. [40]	CNT + glutaraldehyde + PEDOT + gold IDE	11.1	-	100 - 500	14.1
Zhuang et al. [36]	Overoxidized Polypyrrole/Graphene + GCE	-	-	0.5 - 10 25 - 1000	94 ± 15

We have shown that our WS_2-COOH nanotube deposits are not conductive at appropriate potentials and can therefore contrary to CNTs, not contribute to the electrochemical signal capture. However, the increased surface area of the nanotubes for improved enzyme loading and the particular interaction with dopamine almost compensates this lack of conductivity.

Experimental

Chemicals

Dopamine hydrochloride 98%, 1,2-Dihydroxybenzene (catechol), Phosphate buffered saline (PBS) tablets, N-Hydroxysuccinimide (NHS) 98%, 4-(Dimethylamino)pyridine (DMAP) and Tyrosinase from mushroom were purchased from Sigma-Aldrich. WS_2 nanotubes were provided by NanoMaterials Ltd (Yavne, Israel). N-(3-Dimethylaminopropyl)-N'-ethylcarbodiimide hydrochloride (EDC) was purchased from Fluka. All chemicals and solvents were of analytical grade and were used as received, without further purification. WS_2-COOH nanotubes were synthesized and characterized as described in [15]. The obtained material was characterized using FT-IR spectroscopy (Figure 6) where the appearance of characteristic peaks, summarized in table 3, indicate the successful grafting of carboxylic acid functions.

Table 3: selected characteristic FT-IR peaks with vibrational modes

Wavenumber (cm^{-1})	FT-IR vibrational modes
3367	O-H stretching
2881	C-H stretching
1747	C=O stretching of carboxylic acid functionality
1467	C-H bends
1360	C-H rocks
1039	C-S stretching
946	O-H stretching of carboxylic acid functions

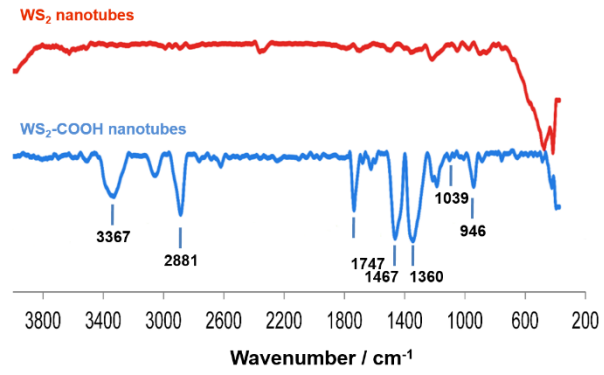

Figure 6: IR spectra of WS2 nanotubes before (top) and after (below) carboxylation.

Moreover and as additional proof for COOH functionalization, characteristic fluorescence-based KAISER tests [41] have been performed after EDC-based derivatization/activation of the polyCOOH shell by 1,3-diaminopropane and ninhydrin reactivity. Fluorescence measurements helped to obtain the optimized carboxylation degree of 0.5 mmol COOH groups g^{-1} of functional WS_2 nanotubes.

Apparatus

FE-SEM images were recorded using an ULTRA 55 FESEM with a GEMINI FESEM column, beam booster (Nanotechnology Systems Division, Carl Zeiss NTS GmbH, Germany), and tungsten gun with an accelerating voltage of 3 kV. The WS_2-COOH deposits were studied in terms of surface roughness and thickness by using a Keyence Vega confocal laser microscope. For this study, WS_2-COOH films were deposited onto a flat gold substrate. In order to determine a representative surface roughness, the images were recorded at low magnifications (×50).

Cyclic voltammetry and Chronoamperometric experiments were performed with an Autolab potentiostat 100 (Eco Chemie, Utrecht, The Netherlands). The data were recorded and operated using Nova software (version 2.1). Modified glassy carbon electrodes (Ø = 3 mm) were used as working electrode for all the characterization. A platinum wire was used as the counter electrode. All electrochemical experiments were carried out using a basic three-electrode cell. A 10^{-2} mol L^{-1} Ag^{+}/Ag electrode was used as a reference electrode in organic media (CH_3CN + 0.1 mol L^{-1} tetrabutylammonium perchlorate, TBAP), whereas a saturated calomel electrode (SCE) was used as a reference electrode in aqueous media.

Prior to any modification, the surface of the glassy carbon electrodes (GCE, ∅ = 3 mm) was polished with a 2 µm diamond paste purchased from Presi (France) and rinsed successively with water, acetone, and ethanol under sonication (5 min). Afterwards, the GCEs were modified with the WS_2-COOH nanotubes. These nanotubes were dispersed by mechanical stirring in distilled water (15 mg of WS_2-COOH in 1L of H_2O). The solution is then allowed to settle for 60 min in order to sediment the larger nanotube clusters. The supernatant was then filtered over cellulose nitrate filter (Sartorius, 0.45 µm, ∅ 3.5 cm) The obtained film was finally transferred to a GCE surface by dissolution of the cellulose nitrate filter according to a procedure described in [23] The same deposition technique was used during laser microscopy characterization, this time using a gold substrate.

Enzyme immobilization on the WS2-COOH nanotube films

The WS_2-COOH nanotube films with a controlled thickness of 6.2 µm, were then used as a support for the immobilization of tyrosinase. This reaction involves the activation of the carboxylic acid functional groups of the film in order to allow the coupling of the NHS function.

Preparation of the WS2-COOH nanotube films

Table 2: Comparison of the obtained characteristics (system used, K_M^{app}, imax, linearity and sensibility) of different nanostructured electrochemical dopamine biosensors.

	System used	K_M^{app} / µmol L^{-1}	i_{max} / µA	Linearity/ µmol L^{-1}	Sensitivity / mA L mol^{-1}
This work	WS_2-COOH nanotube + GCE	41 ± 2	4 ± 0.5	0.5 - 10 10 - 40	6.2 ± 0.7 3.4 ± 0.4
Bujduveanu et al. [34]	CNT + $CaCO_3$ nanoparticules + GCE	30	-	0.015 - 30	250
Wang et al. [39]	SiO_2 nanoparticule+ acide phytic + GCE (laccase)	-	-	0.99 - 103.1	1.9
Lete et al. [40]	CNT + glutaraldehyde + PEDOT + gold IDE	11.1	-	100 - 500	14.1
Zhuang et al. [36]	Overoxidized Polypyrrole/Graphene + GCE	-	-	0.5 - 10 25 - 1000	94 ± 15

For this, the electrode is incubated with PBS (75 µL) containing EDC (20 mmol L^{-1}), NHS (10 mmol L^{-1}) and DMAP (10 mmol L^{-1}) for 12 h at 4°C. EDC and DMAP serve as activation agents. Eventually, the GCE is incubated with a solution containing the concentration of 0.3 mg mL^{-1} of tyrosinase in PBS 0.1 mol L^{-1} pH 7.4 for 12h at 4°C in order to immobilize the enzyme. This enzyme concentration was chosen after a short optimization procedure using 0.1, 0.3, and 0.5 mg mL^{-1} tyrosinase concentration in a cyclic voltammetric setup. The reduction peak currents at -0.1 V vs SCE were recorded in 0.1 molL^{-1}PBS; pH 7.4, containing 5 µmol L^{-1} catechol. Figure 7 shows the obtained values revealing an optimal concentration of 0.3 mgmL^{-1}.

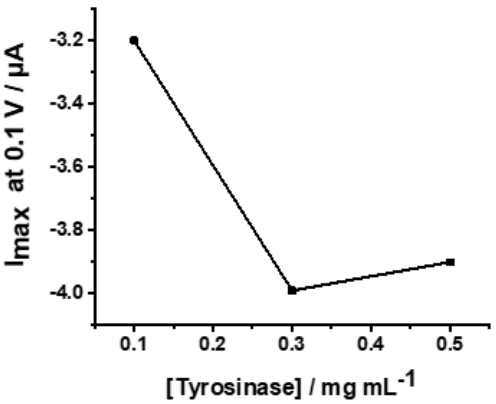

Figure 7: Plot of the peak currents at -0.1 V *versus* different tyrosinase concentration from 0.1 to 0.5 mg mL^{-1}.

The resulting electrodes were then washed carefully several times with PBS solution.

Conclusions

COOH functionalized WS_2 nanotubes were used as platform for enhanced immobilization of the tyrosinase enzyme leading to a catechol and a dopamine biosensor with very satisfying performances. Despite the lack of conductivity of this semiconductor material at appropriate redox potentials for amperometric biosensor applications, these tubes form highly porous deposits with improved enzyme wiring capacities. The determined K_M^{app} values of immobilized tyrosinase are close to the values for the enzyme in solution which represents optimal accessibility of the target molecules to the active site of the enzyme. For dopamine detection, we observed an accumulation of the enzymatically produced dopamine o-quinone leading to enhanced signals at low analyte concentration. The possibility to functionalize these WS_2 nanotubes with carboxylic acid functions make this material easier to process and facilitate post functionalization. At the current state of research, these WS_2-COOH nanotubes provide not superior properties, compared to other described nanomaterials, for electrochemical biosensing applications but they can become promising components in electrochemical biosensor setups as additives due to the sown beneficial properties.

Conflicts of interest

There are no conflicts to declare.

Acknowledgements

We gratefully acknowledge the University Grenoble Alpes (Contrats Doctoraux thématiques UJF 2014) for the PhD fellowship funding of Quentin Palomar, the CNRS PICS program 6344 France Israel for further support. The authors wish also to acknowledge the support from the platform Chimie NanoBio ICMG FR 2607 (PCN-ICMG), from the LabEx ARCANE (ANR-11-LABX-0003-01 and CBH-EUR-GS, ANR-17-EURE-0003), and from the Institut Carnot PolyNat (CARN 0007-01).

Notes and references

1. M. Holzinger, A. Le Goff and S. Cosnier, *Sensors*, 2017, **17**, 1010.
2. P. Mehrotra, *Journal of Oral Biology and Craniofacial Research*, 2016, **6**, 153-159.
3. X. Jia, S. Dong and E. Wang, *Biosensors and Bioelectronics*, 2016, **76**, 80-90.
4. N. Yang, X. Chen, T. Ren, P. Zhang and D. Yang, *Sensors and Actuators B: Chemical*, 2015, **207, Part A**, 690-715.
5. C.-M. Tîlmaciu and M. C. Morris, *Frontiers in Chemistry*, 2015, **3**, 59.
6. E. Morales-Narváez, L. Baptista-Pires, A. Zamora-Gálvez and A. Merkoçi, *Advanced Materials*, 2017, **29**, 1604905-n/a.
7. Y. Song, Y. Luo, C. Zhu, H. Li, D. Du and Y. Lin, *Biosensors and Bioelectronics*, 2016, **76**, 195-212.
8. M. Pumera and A. H. Loo, *TrAC Trends in Analytical Chemistry*, 2014, **61**, 49-53.
9. X. Sun, J. Fan, C. Fu, L. Yao, S. Zhao, J. Wang and J. Xiao, *Scientific Reports*, 2017, **7**, 10290.
10. D. Sarkar, W. Liu, X. Xie, A. C. Anselmo, S. Mitragotri and K. Banerjee, *ACS Nano*, 2014, **8**, 3992-4003.
11. N. Rohaizad, C. C. Mayorga-Martinez, Z. Sofer and M. Pumera, *ACS Applied Materials & Interfaces*, 2017, **9**, 40697-40706.
12. Y. Q. Zhu, W. K. Hsu, N. Grobert, B. H. Chang, M. Terrones, H. Terrones, H. W. Kroto, D. R. M. Walton and B. Q. Wei, *Chemistry of Materials*, 2000, **12**, 1190-1194.
13. N. M., G. A. and R. C. N. R., *Advanced Materials*, 2001, **13**, 283-286.
14. S. Barua, H. S. Dutta, S. Gogoi, R. Devi and R. Khan, *ACS Applied Nano Materials*, 2018, **1**, 2-25.
15. D. Raichman, D. A. Strawser and J.-P. Lellouche, *Nano Res.*, 2015, **8**, 1454-1463.
16. D. Raichman, D. Strawser and J.-P. Lellouche, *Inorganics*, 2014, **2**, 455.
17. W. Z. Teo, E. L. K. Chng, Z. Sofer and M. Pumera, *Chemistry – A European Journal*, 2014, **20**, 9627-9632.
18. J. Laloy, H. Haguet, L. Alpan, D. Raichman, J.-M. Dogné and J.-P. Lellouche, *Nano Convergence*, 2018, **5**, 31.
19. N. Schweigert, A. J. B. Zehnder and R. I. L. Eggen, *Environmental Microbiology*, 2001, **3**, 81-91.
20. H. Fiege, H. Voges, T. Hamamoto, S. Umemura, T. Iwata, H. Miki, Y. Fujita, H. Buysch, D. Garbe and W. Paulus, in *Ullmann's Encyclopedia of Industrial Chemistry*, 2000, DOI: doi:10.1002/14356007.a19_313.
21. G. Lunardi, S. Galati, D. Tropepi, V. Moschella, L. Brusa, M. Pierantozzi, A. Stefani, S. Rossi, F. Fornai, E. Fedele, P. Stanzione, A. H. Hainsworth and A. Pisani, *Parkinsonism & Related Disorders*, 2009, **15**, 383-389.
22. Y. Tao, Y. Lin, J. Ren and X. Qu, *Biosensors and Bioelectronics*, 2013, **42**, 41-46.
23. Q. Palomar, C. Gondran, M. Holzinger, R. Marks and S. Cosnier, *Biosens. Bioelectron.*, 2017, **97**, 177-183.
24. J. Bonde, P. G. Moses, T. F. Jaramillo, J. K. Nørskov and I. Chorkendorff, *Faraday Discussions*, 2009, **140**, 219-231.
25. L. Cheng, W. Huang, Q. Gong, C. Liu, Z. Liu, Y. Li and H. Dai, *Angewandte Chemie International Edition*, 2014, **53**, 7860-7863.
26. S. Cosnier, J. J. Fombon, P. Labbé and D. Limosin, *Sensors and Actuators B: Chemical*, 1999, **59**, 134-139.
27. S. Cosnier and I. C. Popescu, *Analytica Chimica Acta*, 1996, **319**, 145-151.
28. J. C. Espín, R. Varón, L. G. Fenoll, M. A. Gilabert, P. A. García-Ruíz, J. Tudela and F. García-Cánovas, *European Journal of Biochemistry*, 2000, **267**, 1270-1279.
29. D. Shan, M. Zhu, E. Han, H. Xue and S. Cosnier, *Biosens. Bioelectron.*, 2007, **23**, 648-654.
30. V. Carralero Sanz, M. L. Mena, A. González-Cortés, P. Yáñez-Sedeño and J. M. Pingarrón, *Anal. Chim. Acta*, 2005, **528**, 1-8.
31. M. N. Karim, J. E. Lee and H. J. Lee, *Biosensors and Bioelectronics*, 2014, **61**, 147-151.

32. V. Sethuraman, P. Muthuraja, J. Anandha Raj and P. Manisankar, *Biosens. Bioelectron.*, 2016, **84**, 112-119.
33. Y. Zhou, L. Tang, G. Zeng, J. Chen, Y. Cai, Y. Zhang, G. Yang, Y. Liu, C. Zhang and W. Tang, *Biosensors and Bioelectronics*, 2014, **61**, 519-525.
34. M.-R. Bujduveanu, W. Yao, A. Le Goff, K. Gorgy, D. Shan, G.-W. Diao, E.-M. Ungureanu and S. Cosnier, *Electroanalysis*, 2013, **25**, 613-619.
35. L.-P. Mei, J.-J. Feng, L. Wu, J.-Y. Zhou, J.-R. Chen and A.-J. Wang, *Biosensors and Bioelectronics*, 2015, **74**, 347-352.
36. Z. Zhuang, J. Li, R. Xu and D. Xiao, *Int. J. Electrochem. Sci.*, 2011, **6**, 2149-2161.
37. X. Liu, Y. Peng, X. Qu, S. Ai, R. Han and X. Zhu, *Journal of Electroanalytical Chemistry*, 2011, **654**, 72-78.
38. B. Rezaei, E. Havakeshian and A. A. Ensafi, *Sensors and Actuators B: Chemical*, 2015, **213**, 484-492.
39. K. Wang, P. Liu, Y. Ye, J. Li, W. Zhao and X. Huang, *Sensors and Actuators B: Chemical*, 2014, **197**, 292-299.
40. C. Lete, S. Lupu, B. Lakard, J.-Y. Hihn and F. J. del Campo, *Journal of Electroanalytical Chemistry*, 2015, **744**, 53-61.
41. E. Kaiser, R. L. Colescott, C. D. Bossinger and P. I. Cook, *Analytical Biochemistry*, 1970, **34**, 595-598.